Biochemical Applications of Nonlinear Optical Spectroscopy

Edited by

Vladislav V. Yakovlev

CRC Press
Taylor & Francis Group
Boca Raton London New York

CRC Press is an imprint of the
Taylor & Francis Group, an **informa** business

CRC Press
Taylor & Francis Group
6000 Broken Sound Parkway NW, Suite 300
Boca Raton, FL 33487-2742

Printed in the United States of America on acid-free paper
10 9 8 7 6 5 4 3 2 1

International Standard Book Number-13: 978-1-4200-6859-7 (Hardcover)

Library of Congress Cataloging-in-Publication Data

Biochemical applications of nonlinear optical spectroscopy / editor, Vladislav Yakovlev.
p. ; cm. -- (Optical science and engineering ; 138)
Includes bibliographical references and index.
ISBN 978-1-4200-6859-7 (hardcover : alk. paper)
1. Laser spectroscopy. 2. Nonlinear optical spectroscopy. 3. Lasers in biology. 4. Lasers in biophysics. 5. Lasers in chemistry. 6. Biochemistry--Technological innovations. I. Yakovlev, Vladislav. II. Title. III. Series: Optical science and engineering (Boca Raton, Fla.) ; 138
[DNLM: 1. Microscopy--methods. 2. Spectrum Analysis. 3. Optics. QD272.S6 B6155 2008]

QP519.9.L37B56 2008
621.36'6--dc22 2008022656

Visit the Taylor & Francis Web site at
http://www.taylorandfrancis.com

and the CRC Press Web site at
http://www.crcpress.com

1 Structural Dynamics and Kinetics of Myoglobin-CO Binding: Lessons from Time-Resolved X-Ray Diffraction and Four-Wave Mixing Spectroscopy

Valerica Raicu, Marius Schmidt, and Michael Stoneman

CONTENTS

I. INTRODUCTION

Structure, function, and dynamics of biomolecules are coupled closely together. It is not only the structure but also the dynamics of the structural properties that enable a protein to perform its function. Consider, for instance, the case of enzymes, which are catalytically active proteins that assist biochemical reactions. By mixing substrate with an active, functional enzyme, the progress of the reaction toward its end can be monitored by using adequate physical methods. Time becomes an important parameter in such experiments. Measuring how the distribution of molecules over discrete states varies as a function of time is equivalent to observing the kinetics of the reaction. There is a fundamental difference between protein dynamics and kinetics. Protein dynamics lies at the base of kinetics and represents a set of structural changes required for a reaction to occur, whereas kinetics is intrinsically statistical. Without protein dynamics there are no structural changes, no catalytic activity, and hence no kinetics.

In the study of protein dynamics and reaction kinetics, heme proteins are of special interest, primarily because much is known about them and also because ligand dissociation and rebinding may be studied in the time domain following excitation with light pulses. Myoglobin (Mb) is most commonly used as a model heme protein, since it presents all the features required for kinetic studies and yet is structurally and functionally simpler than other proteins, such as hemoglobin. In 1958, myoglobin became the first protein whose structure was determined (Kendrew et al. 1958), and almost 40 years later it became also the first protein to be investigated by nanosecond time-resolved crystallography (Srajer et al. 1996). Its biological role is to bind O_2 and CO_2 in the muscles, but in most dynamic studies of Mb-ligand recombination, CO is used as a ligand, since it can be easily dissociated using light. Also, heme Fe easily oxidizes *in vitro* in MbO_2, which is thus unstable, unlike MbCO.

Figure 1.1 shows the molecular structure of myoglobin consisting of eight α-helical segments wrapped around the functional heme chromophore. Here, carbon-monoxide (CO) is bound to the heme iron. However, this bond can be ruptured by an intense laser flash and the structure starts to relax to the deoxy form.

Obvious questions, such as what the timescales and the structural bases of the relaxations are, where the CO is located, and what the intermediate states of the protein as it progresses toward ligand rebinding are, can be answered by linear and nonlinear laser spectroscopy and time-resolved crystallography.

In this chapter, we first review some of the basic theory of reaction kinetics as well as knowledge accumulated over the past three decades on MbCO recombination kinetics and associated protein motions. Then we present a nonlinear optical technique used in studies of MbCO dynamics and kinetics, the *transient phase grating*. In discussing the results, we focus our attention on the kinetics of protein-ligand recombination, while leaving aside most of the details of segmental motion in proteins during ligand

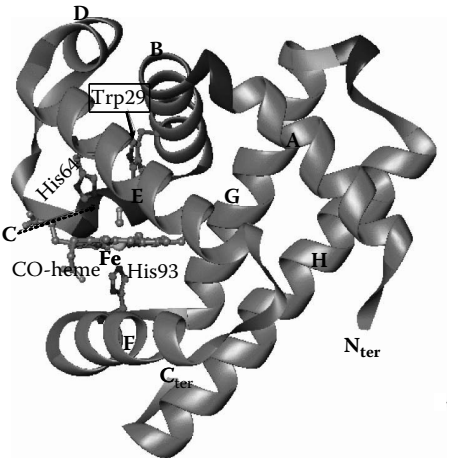

FIGURE 1.1 The architecture of myoglobin. 8 α-helices (A–H) accommodate a heme group, which is attached to the protein via the proximal His93. CO is bound to the iron (Fe) on the distal side of the heme. Here the L29W mutant (Nienhaus et al., 2005) is depicted with the bulky Trp29 bound to helix B on the distal heme side. Figure prepared with "ribbons" (Carson et al. 1997).

dissociation and rebinding. While taking note of the existence of various interpretations of experimental data and competing theoretical models, we only adopt particular interpretations wherever the discussion of experimental data seems to demand it.

II. THEORY OF TRANSIENT STATE KINETICS AND DYNAMICS

A. Systems with a Small Number of Discrete States

Since proteins are essentially polymers, they may adopt many, almost iso-energetic and very similar structures called protein substates (Austin et al. 1975; Frauenfelder et al. 1988). At ambient temperatures, proteins switch between their substates; hence, they are constantly changing their structure (Parak et al. 1982; Parak 2003). By knowing the coordinates of each of the atoms and their velocity vectors at any instant of time, the dynamics of the structural changes, i.e., the trajectories of the molecule's atoms, can be followed exactly. However, this has been achieved only in computer simulations so far.

At thermal equilibrium, a protein may reach a state of minimal energy. If a ligand binds to it, another structure is energetically favored and the protein starts to relax toward it. It is the protein dynamics that couples to the heat bath and enables the molecules to surmount the barriers of energy, which otherwise would prevent the reaction from progressing. Since kinetics is the result of the underlying dynamics, to observe kinetics, an ensemble of reacting molecules is required.

Consider the simple two-state diagram of protein molecules reacting from state A to state B sketched in Figure 1.2. State A is occupied by an ensemble of molecules

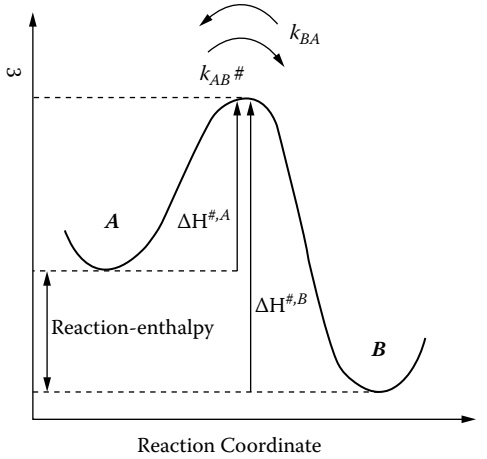

FIGURE 1.2 Two-state diagram (states *A* and *B*) to describe chemical kinetics. The reaction coordinate can be considered as the pathway with lowest energy through the multidimensional energy hyper-surface of the reaction. # represents the transition state, i.e., the state with highest free energy on the reaction coordinate. The reaction enthalpy and the enthalpy differences between the two states and the transition state are depicted by arrows. Note that for the rate coefficients k_{AB} and k_{BA} the free energy differences, including enthalpy and entropy differences, have to be considered.

that undergo complex internal motions individually and independently. There is a finite probability that they will reach the top of the barrier of activation, which is the transition state number (Eyring 1935; Cornish-Bowden 1999), and may relax to state *B*. Measuring the progressively smaller occupancy of state *A* is equivalent to monitoring the kinetics of that reaction. On the other hand, measuring the trajectory of each of the molecules within the states and across the barrier is equivalent to probing the dynamics. At this point, the conceptual difference between kinetics and dynamics becomes clearer.

The reaction rate (or the velocity), which is defined as the change of concentration of a particular species (or protein state), may also be defined as the number of molecules per unit time crossing the barrier from state *A* to *B*. It depends on the height of the barrier, the number of molecules available in state *A*, and the temperature *T*. The height of the barrier and the temperature dependence are parameterized by the rate coefficient, *k*, defined as

$$k = \Omega \cdot e^{\frac{-\Delta H^{\#} + T\Delta S^{\#}}{k_B T}} = \Omega \cdot e^{\frac{-\Delta G^{\#}}{k_B T}} \tag{1.1}$$

where $\Delta G = \Delta H - T\Delta S$ is the Gibbs free energy, Ω may be interpreted as the number of trials per unit time the molecules attempt to jump over the barrier, and the exponential term is the probability that they succeed. This probability depends on the enthalpy of activation, $\Delta H^{\#}$, the entropy difference, $\Delta S^{\#}$, between the states *A* (or *B*) and the transition state #, the Boltzmann constant, k_B, and, of course, the temperature.

It should be pointed out at this juncture that a reaction with no enthalpy of activation ($\Delta H^{\#} = 0$) can nevertheless have a very small rate coefficient, since the entropy of the transition state can be very small compared to that in the state *A* or *B*. Accordingly, $\Delta S^{\#}$ becomes negative. In other words, there is a possibility that only a small loophole or a very narrow path in conformational space exists through which molecules may migrate from state *A* to *B* or vice versa.

If the free energy of the reaction from *A* to *B* has a large negative value, the reaction is irreversible, and the backwards reaction from *B* to *A* can be neglected, since k_{BA} is extremely small. The kinetics is then described by the following simple differential equations:

$$\frac{dA}{dt} = -k_{AB}A, \tag{1.2a}$$

$$\frac{dB}{dt} = k_{AB}A\cdot \tag{1.2b}$$

The temporal derivatives on the right-hand sides represent the changes in concentration of molecules in state *A* or *B*, which are the rates or the velocities of the reaction(s). The second equation follows immediately from Equation (1.2a) and the independent requirement that $A(t) + B(t) = \text{const}$ (i.e., the conservation of mass). The rate is negative when molecules leave a state and positive when they populate a state. In addition, the rate is considered proportional to the concentration of molecules in state *A*. Hence, the larger the number of molecules in state *A*, the larger the velocity of the reaction. Integration of Equation (1.2a) shows that the molecules in *A* vanish according to simple exponential law,

$$A(t) = A_0 e^{-k_{AB}t}, \tag{1.3a}$$

while the population in state *B* increases as

$$B(t) = A_0(1 - e^{-k_{AB}t}), \tag{1.3b}$$

where A_0 is the concentration of molecules in state *A* at the beginning of the reaction, when the concentration of *B* is zero (i.e., $B_0 = 0$). The functions $A(t)$ and $B(t)$ are called "the concentration profiles of the reaction."

If the free energy of the reaction is small, the reaction is reversible. Then the change in the concentration of molecules in state *A* depends on the efflux of molecules from *A* to *B and* the influx of molecules from *B* into *A*. Similar arguments hold for the flux of molecules into and from state *B*. The differential equations are then coupled,

$$\frac{dA}{dt} = -k_{AB}A + k_{BA}B, \tag{1.4a}$$

$$\frac{dB}{dt} = \quad k_{AB}A - k_{BA}B. \tag{1.4b}$$

Equations (1.4a) and (1.4b) can be written using matrix notation as

$$\begin{pmatrix} \frac{dA}{dt} \\ \frac{dB}{dt} \end{pmatrix} = \begin{pmatrix} -k_{AB} & k_{BA} \\ k_{AB} & -k_{BA} \end{pmatrix} \begin{pmatrix} A \\ B \end{pmatrix}, \tag{1.5}$$

or, in a compressed form, as

$$\frac{\boldsymbol{dA}}{\boldsymbol{dt}} = \boldsymbol{KA}\,, \tag{1.6}$$

where $\boldsymbol{A}$ is a vector with the components A and B, $d\boldsymbol{A}/dt$ is its derivative with respect to time, and $\boldsymbol{K}$ is the coefficient matrix. It may be shown that the coupled differential equations can be integrated by finding the eigenvalues and eigenvectors of the coefficient matrix $\boldsymbol{K}$ (Steinfeld et al. 1989). The results again take exponential forms:

$$A(t) = \frac{A_0}{k_{AB} + k_{BA}} \left[k_{BA} + k_{AB} e^{-(k_{AB}+k_{BA})t} \right], \tag{1.7a}$$

$$B(t) = \frac{k_{AB} A_0}{k_{AB} + k_{BA}} \left[1 - e^{-(k_{AB}+k_{BA})t} \right]. \tag{1.7b}$$

Equation (1.6) was solved by assuming that at the beginning of the reaction only state A is occupied with the concentration A_0 and state B is empty. The eigenvalues of this problem are 0 and $-(k_{AB} + k_{BA})$. Note, that the exponents in Equations (1.7a) and (1.7b) both have the same relaxation time, $\tau = 1/(k_{AB} + k_{BA})$. This can be generalized. The observed relaxation times are the inverse of the eigenvalues of the coefficient matrix describing the mechanism (Steinfeld et al. 1989). The number of observable relaxation times is equal to the number of states minus 1 (Matsen and Franklin 1950; Fleck 1971; Henry and Hofrichter 1992). Concentration profiles can be easily determined by numerical methods for any form of the coefficient matrix derived from any mechanism. Figure 1.3 shows concentration profiles for a reaction mechanism employing four states, the initial state and three intermediate states, during a reaction. As expected, three relaxation times are observable.

Any change in the catalytic properties of the protein will change the rate coefficients, k, which in turn will change the concentration profile and the relaxation times. Transient state kinetics becomes a tool to investigate the catalyst. In extreme cases the reaction will stop at some stage and the protein ceases to work. Then, a potent inhibitor might have been found that blocks one of the four states of this reaction. This lies at the base of any kinetic investigation.

B. Distribution of Barrier Heights

Oftentimes, the concentration profile follows neither a simple exponential in time nor a discrete combination of exponentials, but a stretched exponential, which is also

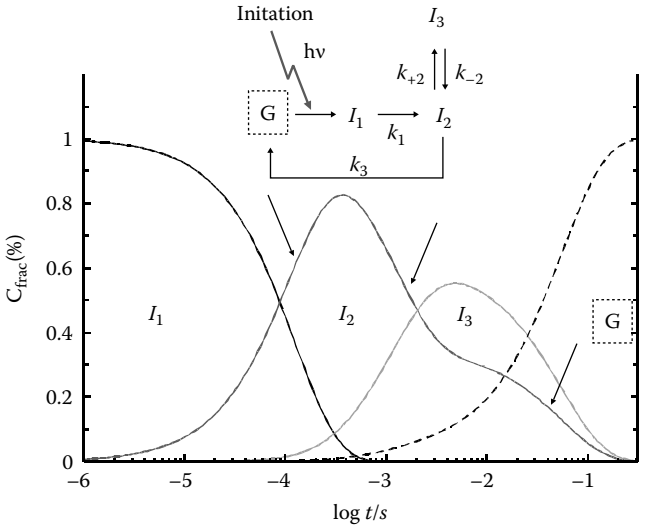

FIGURE 1.3 Concentration profile from a mechanism employing three intermediates, I_1, I_2, I_3, plus the initial (dark) state I_0. $I_1(0) = 1$ is assumed. The cyclic reaction is started (initiated) by a laser flash. Molecules relax through the intermediate states back to the initial state. The concentration profile of intermediate I_2 shows all three relaxation times (arrows).

called the Kohlrausch-Williams-Watt (KWW) equation,

$$A(t) = A_0 e^{-(k_{AB}t)^{\beta}} = A_0 e^{-\left(\frac{t}{\tau_{AB}}\right)^{\beta}}, \tag{1.8}$$

which can cover several decades in time. The power, β, of the exponent is the stretching constant and takes values over the interval [0,1]. If the concentration profile traces a straight line in a log-log representation, it is described by a "power-law" function,

$$A(t) = A_0(1 + k_{AB}t)^{\alpha-1} = A_0\left(1 + \frac{t}{\tau_{AB}}\right)^{\alpha-1}. \tag{1.9}$$

To retain the analogy with a simple exponential function, it is considered in the cases described by Equations (1.8) and (1.9) that there is a distribution of barrier heights, $g(G)$, each height corresponding to an exponential relaxation (Austin et al. 1975; Nagy et al. 2005). The concentration profile is in this case described by

$$A(t) = \int_0^{\infty} g(G_{AB}) e^{-k_{AB}t} dG_{AB}, \tag{1.10}$$

where $g(G_{AB})$ represents the probability of finding a molecule with activation energy between G_{AB} and $G_{AB} + dG_{AB}$. If we assume that Ω is independent of G, Equation (1.1) gives

$$dG_{AB} = -k_B T \frac{dk_{AB}}{k_{AB}}, \tag{1.11}$$

and Equation (1.10) becomes

$$A(t) = k_B T \int_0^{\Omega} \frac{g(k_{AB})}{k_{AB}} e^{-k_{AB}t} dk_{AB}. \tag{1.12}$$

where $g(k_{AB})$ is the distribution of rate constants.

By using the normalization condition for the distribution of relaxation times,

$$k_B T \int_0^{\Omega} g(k_{AB}) dk_{AB} = 1$$

Equation (1.12) may be rewritten as

$$A(t) = \frac{\int_0^{\Omega} \frac{g(k_{AB})}{k_{AB}} e^{-k_{AB}t} dk_{AB}}{\int_0^{\Omega} \frac{g(k_{AB})}{k_{AB}} dk_{AB}} = \frac{\int_0^{\Omega} g(k_{AB}) e^{-k_{AB}t} d(\ln k_{AB})}{\int_0^{\Omega} g(k_{AB}) d(\ln k_{AB})}, \tag{1.13}$$

which expresses the concentration as a fraction of a maximum value.

Expressed in terms of the distribution of relaxation times, $g(\tau_{AB})$, Equation (1.13) reads

$$A(t) = \frac{\int_{\tau_{\min}}^{\infty} \frac{g(\tau_{AB})}{\tau_{AB}} e^{-\frac{t}{\tau_{AB}}} d\tau_{AB}}{\int_{\tau_{\min}}^{\infty} \frac{g(\tau_{AB})}{\tau_{AB}} d\tau_{AB}} = \frac{\int_{\tau_{\min}}^{\infty} g(\tau_{AB}) e^{-\frac{t}{\tau_{AB}}} d(\ln \tau_{AB})}{\int_{\tau_{\min}}^{\infty} g(\tau_{AB}) d(\ln \tau_{AB})}, \tag{1.14}$$

where $\tau_{\min} = 1/\Omega$. Since in most practical circumstances, the largest relaxation time has to be a finite number, the upper limit in Equation (1.13) may be replaced by some $\tau_{\max}$. Hence,

$$A(t) = \frac{\int_{\tau_{\min}}^{\tau_{\max}} \frac{g(\tau_{AB})}{\tau_{AB}} e^{-\frac{t}{\tau_{AB}}} d\tau_{AB}}{\int_{\tau_{\min}}^{\tau_{\max}} \frac{g(\tau_{AB})}{\tau_{AB}} d\tau_{AB}} = \frac{\int_{\tau_{\min}}^{\tau_{\max}} g(\tau_{AB}) e^{-\frac{t}{\tau_{AB}}} d(\ln \tau_{AB})}{\int_{\tau_{\min}}^{\tau_{\max}} g(\tau_{AB}) d(\ln \tau_{AB})}. \tag{1.15}$$

If entropy changes are negligible, one usually speaks of enthalpic barrier heights that the reaction has to overcome. The distribution of relaxation times or rate constants in this case may be equivalently considered a distribution of reaction barrier heights.

A distribution of relaxation times has been proposed (Raicu 1999) that encompasses all known types of relaxation functions (i.e., concentration profiles) when introduced

into Equation (1.15). A convenient particular form of this distribution reads

$$g(\tau_{AB}) = \frac{1}{2\pi} \frac{\left(\frac{\tau_{AB}}{\tau_p}\right)^{\alpha} \sin[\pi(1-\beta)] + \left(\frac{\tau_{AB}}{\tau_p}\right)^{1-\beta} \sin[\pi\alpha]}{\cosh\left[(1-\alpha-\beta)\ln\left(\frac{\tau_{AB}}{\tau_p}\right)\right] + \cos[\pi(1-\alpha-\beta)]} \tag{1.16}$$

where τ_p is the most probable relaxation time, and $0 \le \alpha, \beta \le 1$ are real constants.

When introduced into Equation (1.15), the distribution given by Equation (1.16) leads, e.g., to the simple exponential form of Equations (1.3a) and (1.3b) for $\tau_{AB} \to \tau_p$ and $\alpha = \beta = 0$, the fractional power-law of Equation (1.9) for $\alpha = 1 - \beta$, as well as to other known functions; this distribution is especially useful when the relaxation follows fractal or self-similar pathways (Raicu et al. 2001), and it allows for almost any conceivable relaxation function to be introduced without a need to formulate complicated theoretical models.

C. What Can Be Measured

The ultimate goal of kinetics studies is the identification of a (unique) chemical kinetic mechanism, which consists of a reaction scheme such as the one shown in Figure 1.3 and the corresponding numerical values of the rate coefficients, *k*, which incorporate entropy and enthalpy differences. This is an inverse problem, since only the concentration profile or, in less favorable conditions, only the relaxation times can be observed, and the reaction mechanism must be deduced from this information. Any experimental method that establishes a connection between the signal and the concentration of molecules can be used to investigate kinetics. However, it is necessary that the method has sufficient time resolution since time is the crucial parameter in kinetic experiments.

Many methods of investigation of protein-ligand binding kinetics that are based on linear processes are of a "pump-probe" type. In this approach an optical pulse, called a "pump," starts a photoreaction (such as dissociation of MbCO into Mb and CO), and its progress is probed a time Δt later. The probe could be, for example, a weak laser pulse, which detects the spectral changes in the heme during the protein-ligand recombination, or an x-ray pulse, which allows determination of the protein structure at a particular instant in time.

Both in linear and nonlinear methods, the minimum time delay accessible to the experimenter is the time resolution, and it is determined by either the duration of the pump or the probe pulse, whichever is longer. Two linear methods are discussed in section II, while a nonlinear method is presented in section IV. Typical timescales for protein catalyzed reactions range in the nanosecond (ns) to millisecond (ms) time range and the time resolution must be much better in order to sample the time range sufficiently. However, there are processes in proteins that are much faster, often occurring at femtosecond (fs) timescales (Franzen et al. 1995; Lim et al. 1993; Jackson et al. 1994; Armstrong et al. 2003; Nagy et al. 2005). To observe these processes,

the time resolution must be exquisite (Norrish et al. 1965). This adds tremendous complication to the experiments.

In the next section, we describe two pump-probe approaches and review their use in experiments with MbCO. This places the nonlinear optical techniques of transient phase grating introduced in the subsequent section in their proper context.

III. PUMP-PROBE STUDIES OF PROTEIN-LIGAND BINDING

A. Experimental Methods

1. Optical Pump-Probe Spectroscopy

In the typical setup, excitation light is provided by a pulsed (e.g., nanosecond) laser (emitting in the visible range, e.g., at 532 nm, if Mb is investigated), while the probe is delivered by a continuous-wave (cw) laser. The two beams are spatially overlapped in the sample, and the temporal changes in the optical properties (such as optical absorption or frequency shift) that follow the passage of the pump pulse are registered by a detector with short response time (relative to time scale of the processes monitored), such as a fast photodiode.

If the processes of interest occur on the nanosecond or longer time scale, one can usually visualize the evolution of the parameter of interest using an oscilloscope. For shorter timescales, standard electronics is too slow, and temporal information is determined by passing the pulsed probe light through a delay line with adjustable length (Nagy et al. 2005). Then, the time coordinate is obtained by dividing the length of the beam path in the delay line by the speed of light.

2. Time-Resolved Crystallography

X-ray crystallography is the method of choice for determination of structures of large macromolecules such as proteins. Nowadays, roughly 48,000 x-ray structures are stored in the Protein Data Bank (http://www.rcsb.org; Berman et al. 2000). X-ray crystallography is traditionally a static method, i.e., without time resolution. In order to follow the kinetics and to determine the structure of the transiently occupied intermediate states of proteins, time-resolved crystallography has to be used (Moffat 1989). The time resolution, t_{min}, has to be as good as for any other method employed to follow reaction kinetics. This implies that x-ray data must be collected as fast as possible.

In third-generation synchrotrons, the x-rays are generated in intense flashes of ~100 picoseconds (ps) duration. If, during this time, an entire diffraction pattern is recorded, the time resolution t_{min} equals 100 ps (Szebenyi et al. 1992; Srajer et al. 1996, Schotte et al. 2003). However, the traditional monochromatic oscillation diffraction method cannot be used since there is no way to rotate the crystal during this 100 ps timeframe to collect the integrated intensity of a Bragg reflection. Still exposures, therefore, have to be used.

Although other methods could be used to determine the integrated intensity, the Laue method (Amoros et al. 1975; Bartunik et al. 1992; Ren et al. 1999) has been the method of choice so far. In this method, the crystal is subjected to a spectrum of x-ray radiation. Each reflection accepts a small fraction of this bandwidth, which covers the entire reflection range of that particular reflection. Hence, the integrated

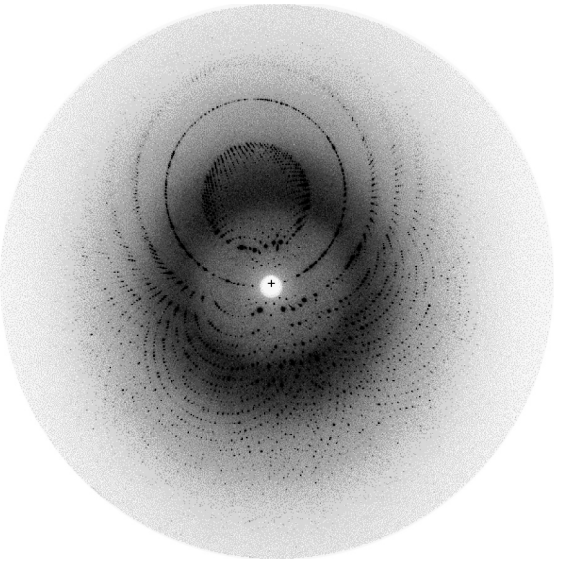

FIGURE 1.4 A protein Laue diffraction pattern.

intensity can be recorded instantaneously without rotating the crystal. This is the sole physical reason for the use of the Laue method. Of practical value is that a substantial fraction of the reciprocal space is sampled with one diffraction pattern (Figure 1.4). Consequently, an entire Laue data set can be collected rapidly. With optimized, polychromatic, synchrotron-based undulator x-ray sources, a number of different crystal settings spaced approximately 2–3 degrees apart cover the unique volume of the reciprocal space.

Using time-resolved crystallographic experiments, molecular structure is eventually linked to kinetics in an elegant fashion. The experiments are of the pump-probe type. Preferentially, the reaction is initiated by an intense laser flash impinging on the crystal and the structure is probed a time delay, Δt, later by the x-ray pulse. Time-dependent data sets need to be measured at increasing time delays to probe the entire reaction. A time series of structure factor amplitudes, $|F_t|$, is obtained, where the measured amplitudes correspond to a vectorial sum of structure factors of all intermediate states, with time-dependent fractional occupancies of these states as coefficients in the summation. Difference electron densities are typically obtained from the time series of structure factor amplitudes using the difference Fourier approximation (Henderson and Moffatt 1971). Difference maps are correct representations of the electron density distribution. The linear relation to concentration of states is restored in these maps. To calculate difference maps, a data set is also collected in the dark as a reference. Structure factor amplitudes from the dark data set, $|F_D|$, are subtracted from those of the time-dependent data sets, $|F_t|$, to get difference structure factor amplitudes, ΔF_t. Using phases from the known, precise reference model (i.e., the structure in the absence of the photoreaction, which may be determined from

static x-ray diffraction), difference structure factors, and corresponding difference maps, $\Delta\rho_t$, are calculated for each time point, t.

Difference electron densities can be globally analyzed by methods from linear algebra, as has been successfully demonstrated in the literature (Schmidt et al. 2003; Schmidt et al. 2004; Rajagopal et al. 2004, 2005; Ihee et al. 2005). At the base of the analysis is a component analysis, the singular value decomposition (***SVD***). It takes a time series of difference maps (matrix $\boldsymbol{A}$) and decomposes it into a set of time-independent, singular difference maps, the left singular vectors $\boldsymbol{U}$ and their respective time courses, the right singular vectors $\boldsymbol{V}$. Matrices $\boldsymbol{U}$ and $\boldsymbol{V}$ are connected by a diagonal matrix $\boldsymbol{S}$, which contains the singular values

$$\boldsymbol{A} = \boldsymbol{U}\,\boldsymbol{S}\,\boldsymbol{V}^T. \tag{1.17}$$

How matrix $\boldsymbol{A}$ is set up and details of the ***SVD*** analysis of time-resolved x-ray data are described elsewhere (Schmidt et al. 2003, 2005b; Schmidt 2008). Essentially the relaxation times of the kinetics are found in a global way in the right singular vectors $\boldsymbol{V}$. By interpreting the kinetics with a suitable chemical kinetic model, it becomes possible to project the left singular vectors onto the intermediate states (Henry and Hofrichter 1992; Schmidt et al. 2003). Basically, this operation linearly combines the content of the singular vectors in a concentration- dependent way. As a result, the time-independent difference electron densities of the intermediates can be found, from which the structures of the intermediates are determined (Schmidt et al. 2004; Rajagopal et al. 2005; Ihee et al. 2005).

B. Pump-Probe Studies of Mb-CO Recombination

The interest in studying the structures of intermediates in myoglobin can be traced back to the groundbreaking work of Frauenfelder and coworkers (Austin et al. 1975). They flashed away the CO and observed the rebinding kinetics at various temperatures spectroscopically. Steps or phases in the kinetics were assumed to correspond to different intermediate states. What do these intermediate states look like? Several possible positions of the CO in the heme pocket were determined independently by three groups in the 1990s using cryo-crystallographic techniques (Schlichting et al. 1994; Teng et al. 1994, 1997; Hartmann et al. 1996). From those experiments, it appeared that the CO molecule can be driven by extended illumination to a distance of up to 3.5 Å from the heme iron (Figure 1.5, B-site). Other positions could not be populated at low temperatures, which required other experimental schemes to be developed (Ostermann et al. 2000; Nienhaus et al. 2005). Results from one of these schemes are described in Figure 1.6.

MbCO L29W mutant crystals are cooled from 180 K to 105 K during laser illumination. The CO is found on the proximal side of the heme. This site is identical to one of the four sites previously characterized by binding xenon (Tilton et al. 1984). They are called Xe1…Xe4 sites (see Figure 1.5 for their approximate positions). Only Xe1 is populated in this experiment. No electron density of the CO is found at the iron-binding site (Figure 1.5, B-site). Subsequent heating followed by structure determination at 105 K show the rebinding of the CO from Xe1 back to the iron.

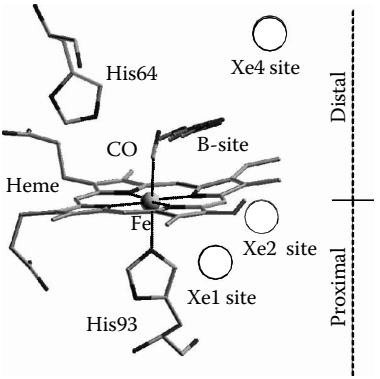

FIGURE 1.5 The heme pocket of myoglobin. B-site: CO found here also at cryogenic temperatures. Xe1…Xe4 sites: identified in xenon binding experiments.

Effective ligand rebinding from the Xe1 site is only observed when the temperature has risen above a characteristic temperature $T_c \sim 180$ K (Figure 1.6), which is the temperature where protein dynamics sets in. However, the time-related information is lost in experiments at cryogenic temperatures. Time-resolved crystallography was applied to restore the time scale and observe undisturbed relaxations.

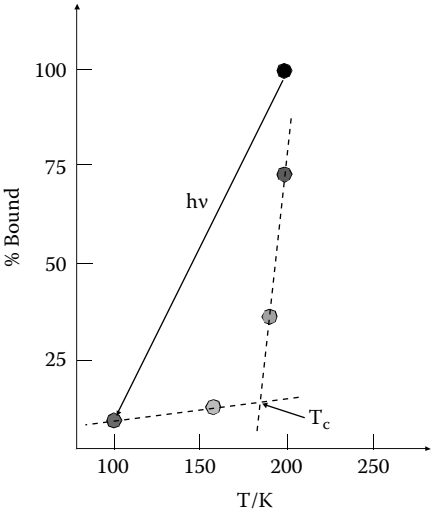

FIGURE 1.6 Photoflash experiments with temperature cycling on L29W MbCO. Amount of CO (occupancy of CO) bound to the iron determined from integrating the electron density at the iron-binding site of the CO. Black circle (a): initial species, not photolyzed. Dark blue circle (b): directly after the crystal was cooled to 105 K under continuous illumination. Light blue circle (c): after warming to 160 K. Green circle (d): after 180 K. Red circle (e) after 200 K. (From Nienhaus, K., Ostermann, A., Nienhaus, U., Parak, F., and Schmidt, M., *Biochemistry* 44: 5095–5205, 2005. With permission.)

Currently, up to four different species of sperm whale myoglobin have been investigated by time-resolved crystallography: the wild-type (Srajer et al. 1996, 2001; Schotte et al. 2004), the L29W mutant (Schmidt et al., 2005a), the L29F mutant (Schotte et al. 2003, 2004) and the YQR triple mutant (Bourgeois et al. 2003, 2006). Table 1.1 shows the positions and timescales on which the CO was discovered in their respective sites. The L29W mutant is unique, since it is the slowest rebinder of all species. Other mutants like the L29F mutant are interesting, since the CO resides a much shorter time interval in the primary docking B as compared to the wild-type. Other cavities such as Xe4 and Xe2 are populated rapidly and the subsequent occupation of these cavities can be followed (Schotte et al. 2003).

In the L29W mutant, the CO could be observed in the Xe1 site 300 ns after the photoflash. No other binding site could be identified even on the fastest times around 1 ns. Xe4 site was most likely dynamically occluded by a bulky tryptophan residue. Even on very fast timescales, the CO stays in Xe1 for an exceptionally long time. Comparison of relevant relaxation times derived from the time-resolved crystallographic data on the L29W mutant and the wild-type made it possible to determine the pathway of the CO out of the myoglobin. Figure 1.7 shows the relaxations observed in the L29W mutant and marks relevant timescales observed in the wild-type. In the wild-type, depopulation of the distal pocket binding site B follows a stretched exponential with $\tau \sim 70$ ns. At the same time, the proximal site Xe1 becomes populated. Xe1 depopulates biphasically on timescales of a few hundred nanoseconds and 100 μs. Rebinding of CO to the iron occurs in concert with the depopulation of Xe1. However, in the L29W the CO stays for 1.5 ms in the proximal Xe1 site. This time scale is much larger than those observed in the wild-type. In addition, in the L29W mutant the CO molecules first

TABLE 1.1
Sites Where CO can be Observed in Photoflash Experiments in Different Species of Sperm Whale Myoglobin (References in the Text)

Species/Site	B	Xe4	Xe2	Xe1
Wild-type[a]	Up to 70 ns	—	—	30 ns to 100 μs
L29W[b]	—	—	—	300 ns to 1.5 ms
L29F[c]	Up to 1 ns	1 ns to 3 ns	3 ns to 30 ns	30 ns to >3 μs
YQR[d]	—	Up to 20 ns	—	20 ns to >3 μs

Notes: Relaxation times are available for the wild-type and L29W mutant. For the L29F and YQR Mb mutants, approximate relaxation times were derived by visual inspection of the difference maps and by inspecting the time course of integrated difference electron densities, respectively.

[a] Data from Srajer, V., Ren, Z., Teng, T. Y., Schmidt, M., Ursby, T., Bourgeois, D., Praderv and, C., Schildkamp, W., Wulff, M., and Moffat, K. 2001. *Biochemistry 40:*13802–15.

[b] Data from Schmidt, M., Nienhaus, K., Pahl, R., Krasselt, A., Nienhaus, U., Parak, F., and Srajer, V. 2005. *Proc. Natl. Acad. Sci. USA* 13:11704–9.

[c] Data from Schotte, F., Lim, M., Jackson, T. A., Smirnov, A. V., Soman, J., Olson, J. S., Phillips, G. N. Jr., Wulff, M., and Anfinrud, P. A. 2003. *Science* 300:1944–47.

[d] Data from Bourgeois, D., Vallone, B., Arcovito, A., Sciara, G., Schotte, F., Anfinrud, P. A., and Brunori, M. 2006. *Proc. Natl. Acad. Sci*. USA 103:4924–29.

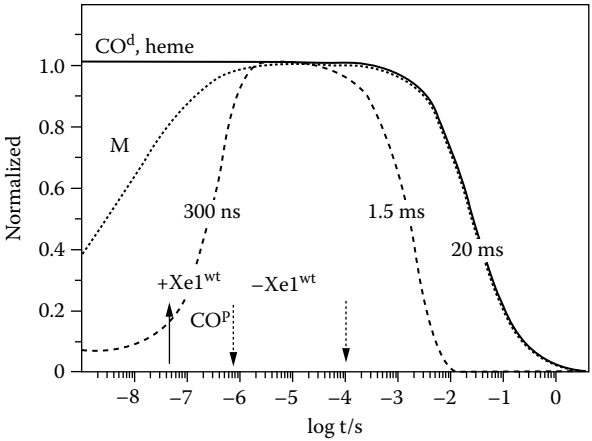

FIGURE 1.7 Rebinding kinetics in the L29W myoglobin. CO^d, heme: instantaneous displacement of bound CO and heme, final relaxation follows CO rebinding with $\tau = 20$ ms. M: protein moieties, initial stretched relaxation, final relaxation follows CO rebinding with $\tau = 20$ ms. CO^p: CO in Xe1 site. In L29W Mb Xe1 is populated with $\tau = 300$ ns and depopulated with $\tau = 1.5$ ms. In the wild-type Xe1 is populated with ~30 ns (solid arrow at $+Xe1^{wt}$) and depopulated biphasically on timescales of ~800 ns and ~100 μs (dashed arrows at $-Xe1^{wt}$). Note the very large time window accessible in the L29W Mb. (From *Proc. Natl. Acad. Sci. USA* 101:4799–4804. Used with permission.)

leave the Xe1 site, most likely to the solvent, before they rebind to the iron with $\tau \sim$ 20 ms. Hence, rebinding is two orders of magnitude slower than in the wild-type. The only structural difference between the myoglobin species is that a leucine at position 29 in the wild-type is replaced by a bulky tryptophan in the L29W mutant. Although Trp29 is on the distal side of the heme, it has a dramatic effect on the migration of CO. Obviously, Trp29 blocks the most important migration pathway. Hence in the L29W the CO has to find another way. As suggested by molecular dynamics simulations, several pathways are conceivable that take advantage of the network of cavities in myoglobin (Cohen et al. 2006). These pathways, however, must be much slower than the pathway on which CO leaves Xe1 in the wild-type. Hence, these pathways are not important for the protein's function. In the wild-type, CO migrates to the solvent through the distal side of the heme, which is not blocked there.

On timescales faster than a few nanoseconds, the relaxation kinetics of the protein structure is non-exponential (Lim et al. 1993; Jackson et al. 1994). This has also been observed with time-resolved crystallography for the YQR triple mutant (Bourgeois et al. 2003, 2006) and for the L29W mutant (Figure 1.7, protein moieties M) (Schmidt et al. 2005a). In this case, the picture of simple kinetics drawn by the two-state model in Figure 1.2 most likely fails. These fast timescales coincide with characteristic timescales of protein-specific motions that range from 10 ps to a few ns in myoglobin (Parak 2003). On these timescales, equilibration between all modes of motion (degrees of freedom) is not achieved and the relaxation of the ensemble is likely observed as diffusive motion along a rough energy surface (Hagen and Eaton 1996). However, at this time, structural models do not exist on ultrafast timescales. To develop structural

and kinetic descriptions for the fastest reactions in proteins, heme proteins will remain one of the future prime targets for time-resolved methods.

IV. NONLINEAR TRANSIENT PHASE GRATING SPECTROSCOPY

A. Experimental

1. General Principles

Two pulsed coherent beams with parallel polarization intersect in the sample at an angle θ_{ex} to form an interference pattern in the material (Figure 1.8). The spatial variation of the intensity along the spatial coordinate x is given by

$$I(x) = \frac{I_m}{2}\left(1 + \cos\frac{2\pi x}{\Lambda}\right), \tag{1.18}$$

where I_m is the maximum intensity and Λ is the fringe spacing of the grating, given by (Nagy et al. 2005; Eichler et al. 1986; Nelson et al. 1982):

$$\Lambda = \frac{\lambda_{ex}}{2\sin(\theta_{ex}/2)}. \tag{1.19}$$

In this equation, $\Lambda = 2\pi/|\mathrm{k}_{ex1} - \mathrm{k}_{ex2}|$, and λ_{ex} is the wavelength of both excitation beams.

The bright fringes of the interference pattern modulate the material optical properties through photoinduced processes to form a diffraction grating in the sample. The probe pulse, incident on the sample at the Bragg angle for diffraction (Θ), diffracts off the grating with an efficiency given by the expression (Eichler et al. 1986; Kogelnik 1969):

$$\eta(\lambda,t) = \zeta(\lambda_p,t)[\Delta n(\lambda,t)^2 + \Delta\kappa(\lambda,t)^2], \tag{1.20}$$

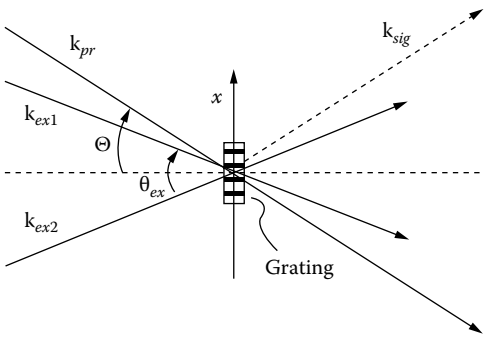

FIGURE 1.8 Phase matching diagram for transient grating experiments. Significance of the symbols: k_{ex1}, k_{ex2} = wave vectors of the excitation beams; k_{pr} = wave vector of the probe beam; k_{sig} = wave vector of the signal (diffracted) beam.

where $\Delta n(\lambda,t)$ and $\Delta\kappa(\lambda,t)$ are changes in the real and imaginary parts of the complex index of refraction ($n^* = n + i\kappa$) of the sample, respectively, and $\zeta(\lambda_p,t)$ is given by

$$\zeta(\lambda_p,t) = G(w,\theta_{ex})\left(\frac{\pi d}{\lambda_p \cos\Theta}\right)^2 \exp\left[\frac{-2.3\alpha(\lambda_p,t)}{\cos\Theta}\right]^2, \tag{1.21}$$

with $G(w,\theta_{ex})$ being a constant factor that depends on the waist (w) and the incidence angle (θ_{ex}) of the Gaussian excitation beams, α the average density at the probe wavelength (λ_p), d the thickness of the grating in the sample, and Θ the Bragg angle of diffraction.

Since the beams are pulsed (usually, at nanosecond level), the grating forms only transiently, i.e., it dissipates within a short time after the passage of the two pulses through the sample. Therefore, the probe senses the ensuing transient dynamics in the sample following formation of the grating and before its dissipation.

As mentioned above, the diffracted signal reports on excitation-induced changes in both the real and the imaginary parts of the index of refraction. Changes in the imaginary part ($\Delta\kappa$) reflect changes in absorption by the sample, while changes in the real part are due to a superposition of mainly three effects, as given by

$$\Delta n = \Delta n_{protein} + \Delta n_{ex} + \Delta n_{th}, \tag{1.22}$$

where $\Delta n_{protein}$ are changes due to the protein dynamics (which is the information sought after in studies of protein dynamics). The third term (Δn_{th}) reflects contributions to the signal arising from density changes due to heating of the sample; it consists of a fast oscillating component with a period of ~1 ns (for liquid samples) and an exponentially decaying part due to thermal diffusion. Both of these components can be identified and/or corrected for (Nagy et al. 2005; Walther et al. 2005). Finally, the second term (Δn_{ex}) and also $\Delta\kappa$ mentioned above are electronic contributions that arise from the absorption differences between the protein and its dissociated state (i.e., between MbCO and deoxy-Mb, in the case of myoglobin) (Ogilvie et al. 2002). These contributions can be dramatically reduced by using an off-resonant probe beam (Ogilvie et al. 2002; Deak et al. 1998). In this way, the transient grating method detects only changes in the real part of the complex index of refraction, which incorporate important information on the protein dynamics.

2. Diffractive Optics-Based Four-Wave Mixing with Heterodyne Detection

The already high sensitivity of the transient grating spectroscopy may be further improved by using optical heterodyne detection. In this method, a relatively weak signal field is mixed with a much more intense coherent field, called a *local oscillator* or *reference field* (such as the beam denoted by "ref1" in Figure 1.9). The experimental setup requires in this case two probe beams, crossing each other in the transient grating at twice the Bragg angle (Figure 1.9). The signal is represented by a small fraction of the probe intensity that is diffracted by the transient grating, such as the

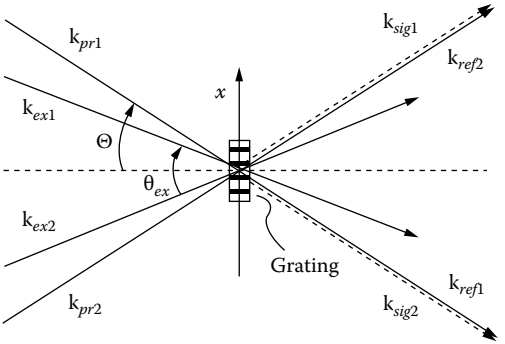

FIGURE 1.9 Schematic representation of the excitation, probe, signal, and reference beams used for heterodyne detection in transient phase grating experiments.

beam characterized by $\boldsymbol{k}_{sig1}$ in Figure 1.9, while the local oscillator is constituted by an intense beam, such as the beam characterized by $\boldsymbol{k}_{ref2}$ in the figure, which is the portion of probe 1 that passes undiffracted through the grating.

The mixing of the signal and reference beams results in a measured intensity that incorporates a strong constant contribution from the reference field $[E_{ref2}(t)]$ and a term that combines the strong reference with the weak signal field (Goodno et al. 1999), as expressed by

$$I_{OHD} = |E_{ref2}(t)|^2 + 2|E_{sig1}||E_{ref2}|\cos(\varphi_{sig1} - \varphi_{ref2}), \tag{1.23}$$

where φ_{sig1} and φ_{ref2} are the phases of the signal and reference fields, respectively, and a term corresponding to the intensity of the signal field ($|E_{sig1}(t)|^2$) has been considered negligibly small. The mixed term retains the phase of E_{sig1} through modulation of the more intense reference field (E_{ref2}), and thereby allows detection of E_{sig1} with a higher signal-to-noise ratio (Levenson and Eesley 1979) compared to the method that measures the signal field directly.

As seen from Figure 1.9, exactly the same procedure may be used for detection of E_{sig2} from mixing the fields of $\boldsymbol{k}_{sig2}$ and $\boldsymbol{k}_{ref1}$.

It can be shown that, under phase-matching conditions, I_{OHD} is related to Δn and $\Delta\kappa$ by the expression (Nagy et al. 2005):

$$I_{OHD} \cong 4n|E_{sig}||E_{ref}|(\Delta n \sin\phi - \Delta\kappa\cos\phi), \tag{1.24}$$

in which the constant term $|E_{ref}(t)|^2$ has been ignored and ϕ has replaced $\varphi_{sig} - \varphi_{ref}$.

Rogers and Nelson outlined the use of a transmission grating for easy alignment of all the beams in transient grating experiments (Rogers and Nelson 1996). Critical refinements, introduced by the group of Miller (Miller 2002; Goodno et al. 1998, 1999) has led to the development of diffractive-optics-based transient grating experiments with heterodyne detection (or diffractive-optics-based four-wave mixing). Besides its inherent simplicity, the technique features very high sensitivity and stability.

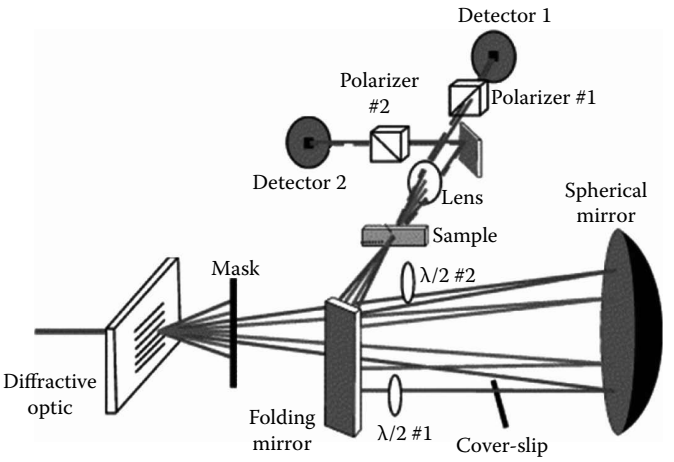

FIGURE 1.10 Schematic representation of the experimental setup for diffractive optics-based four-wave mixing with heterodyne detection. (From Ogilvie, J. P., Plazanet, M., Dadusc, G., and Miller, R. J. D. 2002. *J. Phys. Chem.* 109:10460–67. With permission)

In the typical setup (Figure 1.10), excitation light is provided by a pulsed (e.g., nanosecond) laser emitting at 532 nm, while the off-resonant probe is delivered by a cw laser (for instance an Nd:YVO laser operating at 1064 nm). The two coherent beams are overlapped using a dichroic mirror and then passed together through a surface relief diffractive optics. A spatial filter (i.e., mask) blocks all but the ± 1-order diffracted beams, which are focused onto the sample by a spherical mirror. The focused excitation beams (532 nm) form a transient grating in the sample, which diffracts the probe beams. The two diffracted beams and the residual probe beams that cross the sample are collimated by a lens and directed in pairs of one diffracted (i.e., signal) and one undiffracted (i.e., reference) beam to two separate fast photodiodes (with rise-time of ~1 ns), which are connected to an oscilloscope. The time-course of the heterodyne signals from each beam pair is recorded separately or differentially. The relative phase [ϕ in Equation (1.22)] between the diffracted and undiffracted beams is adjusted by tilting a cover slip in the path of one of the probe beams before entering the sample. This ensures easy separation of the real part of the signal (i.e., Δn) from the imaginary part ($\Delta\kappa$) (Ogilvie et al. 2002, Walther et al. 2005), and a further increase in the signal-to-noise ratio.

B. Overview of Transient Grating Results

1. MbCO in Aqueous Solutions

In aqueous solutions at room temperature, the bond-breaking event is usually followed by ligand escape from the protein. Rebinding requires that the ligand overcomes a series of barrier heights beginning with the first step of repenetrating the protein. The ligand motion through the protein requires that the protein as a whole

undergoes a series of structural changes that facilitate motion of CO away from the heme following photoflash and then back until the final event of rebinding occurs (Ogilvie et al. 2001; Dadusc et al. 2001; Sakakura et al. 2001). As mentioned above, x-ray crystallography suggests that ligand escape is guided through a few specific internal cavities; these are presumably open and closed by fluctuations in the protein conformations. Ligand motion through the protein must therefore be accompanied by protein volume changes (ΔV) or development of material strain ($\Delta V/V$) due to protein deformation to accommodate the unbound ligand (Dadusc et al. 2001)

Phase grating spectroscopy provides exquisite sensitivity for monitoring volume changes in the protein, which are reflected by changes in the index of refraction [see Equations (1.21) and (1.22)]. Figure 1.11 shows the time changes in the real part of the refractive index obtained from transient phase grating measurements on MbCO following photo-induced bond breaking (Ogilvie et al. 2001; Dadusc et al. 2001).

Several features can be distinguished in Figure 1.11. First, a peak is observed within the first tens of nanoseconds (region I, in Figure 1.11), which has been ascribed to structural birefringence (Dadusc et al. 2001). The increase in the index of refraction suggests protein contraction. The barely perceptible plateau followed by the large decay (region II) that induces a sign change in the signal were assigned to CO motions inside the protein; region II may be divided into two subregions, corresponding to CO transition between two intermediate cavities inside the protein and between one of the cavities and the solvent, respectively (Dadusc et al. 2001). However, the time scale of phase II coincides with the time scale identified in time-resolved crystallographic experiments on various myoglobin species (Schmidt et al. 2005a; Bourgeois et al. 2003, 2006). Processes occurring at this time scale have been associated with structural relaxation from an energetically unfavorable deoxy species formed shortly after Fe-CO bond breaking toward the equilibrium of the deoxy-Mb species. Since the transient grating experiment is sensitive to structural

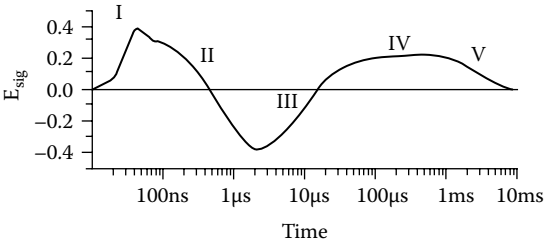

FIGURE 1.11 Changes in the real part of the refractive index following photodissociation of MbCO (in arbitrary units). Recall that the real part of the index of refraction probe's volume changes in the whole protein and is insensitive to the optical absorption of the heme. Various regions are marked in the figure by Roman numerals and the underlying physical mechanisms are identified in the text. The transient grating has been created in the sample by using a 20-ns laser pulse at 527 nm, and the volume changes have been probed by a cw beam at 1064 nm. (From Ogilvie, J. P., Armstrong, M. R., Plazanet, M., Dadusc, G., and Miller, R. J. D. 2001. *J. Luminesc.* 94–95:489–92. With permission.)

changes of the entire protein, it is conceivable that most of the signal of phase II in Figure 1.11 is due to this structural relaxation. Changes in region III are due to slower relaxation dynamics and are dominated by the thermal diffusion of the grating, while the further slower increase in the signal in region IV has been assigned to CO diffusion out of the grating (Dadusc et al. 2001). Finally, the bimolecular recombination (i.e., recombination of CO with a different Mb molecule) is responsible for the decrease in signal in region V toward zero, and the protein is ready for a new dissociation-recombination cycle induced by a new transient grating.

For further discussion of the above results, and for correlations with existing pump-probe data as well as with other techniques, the reader is referred to original papers (e.g., Ogilvie et al. 2001, 2002 Dadusc et al. 2001; Sakakura et al. 2001) as well as to a recent review by Nagy et al. (2005).

2. Non-Exponential Kinetics and Dynamics of MbCO in a Glass

Low-temperature measurements, especially of flash photolysis, have revealed very complicated kinetics, especially non-exponential dependence on time, of Mb-CO recombination when the temperature goes below the glass transition temperature of the surrounding medium (Austin et al. 1975; Srajer et al. 1988; Tian et al. 1992; Lim et al. 1993; Hagen and Eaton, 1996). This behavior deviates markedly from simple exponential forms observed at room temperature. A possible explanation has been proposed that below the glass-transition temperature proteins are "frozen" in various conformational substates, characterized by a broad distribution of enthalpic barrier heights (Austin et al. 1975; Frauenfelder et al. 1988; Steinbach et al. 1991), each height corresponding to an individual substate. Accordingly, this leads to the non-exponential time dependence of the rebinding kinetics observed experimentally. At room temperature, proteins are assumed to change their conformations on timescales much faster than binding occurs, so that these fluctuations are averaged out. An average reaction rate constant is obtained, which leads to the observed exponential behavior. We note that general agreement on the detailed interpretation of non-exponential kinetics has yet to be reached (see, e.g., Frauenfelder et al. 1988; Hagen and Eaton 1996; Parak 2003; Ye et al. 2007), for various views regarding this issue).

Much of the work on Mb-CO recombination following photodissociation has been devoted to the study of *geminate* recombination (i.e., rebinding to the same heme of the CO molecules trapped inside protein pockets), and in particular to whether rebinding kinetics couples to the outer protein motions. In their papers on the effect of viscosity on the rapid conformational changes in the protein following photodissociation, Ansari et al. suggested that protein relaxation may slow down the geminate recombination and increase barrier heights for ligand rebinding to Mb in high-viscosity solvents at room temperature (Ansari et al. 1992, 1994). Based on an extrapolation of their results to high viscosities, those authors suggested that a sufficiently viscous solvent should suppress protein relaxation as well as the interconversion of conformational substates. Similar to what happens at low temperatures in aqueous solvents, this viscosity effect should then lead to non-exponential rebinding kinetics. This prediction has been confirmed experimentally in studies of MbCO

embedded in a room-temperature trehalose glass (Hagen et al. 1995, 1996), although interpretation of those results in terms of coupling between heme-protein motions has been questioned by other authors (Sastry and Agmon 1997).

In a recent paper by Walther et al. (2005), the ability of the trehalose glass to prevent large protein relaxations at room temperature has been used to determine the binding energy of the CO group to the heme of Mb. A binding energy of ~34 kcal/mol has been observed, which agrees with molecular dynamics simulations (Rovira and Parrinello 2000).

Analysis of pump-probe absorption data of Walther et al. (2005; not shown here) indicated two stretched exponentials characterizing the geminate recombination. In agreement with pump-probe results, their transient grating data (reproduced in Figure 1.12) have been fitted by an equation,

$$\mathrm{Re}(I_{OHD}) = \left\{ A_{th} + A_{th1}\left[1 - e^{(k_1 t)^{\beta_1}}\right] + A_{th2}\left[1 - e^{(k_2 t)^{\beta_2}}\right] \right\} e^{-t/\tau_{th}}, \qquad (1.25)$$

which incorporates two stretched exponentials corresponding to two distinct geminate processes (subscripts "1" and "2") and a simple exponential (without subscript) accounting for the thermal grating decay. Very similar values for τ_{th} have been

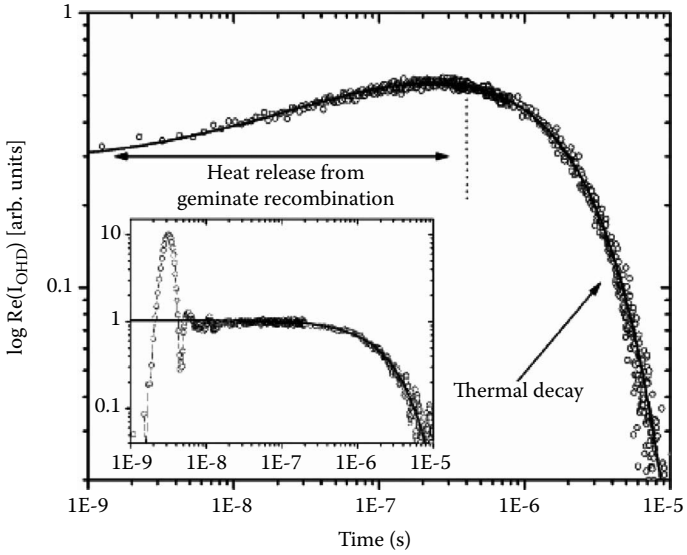

FIGURE 1.12 Measured diffraction grating signal (in arbitrary units) of MbCO embedded in a trehalose glass at room temperature (*open circles*) and theoretical simulation using equation (25) (*solid line*). The fitting parameters corresponding to the best-fit curve are $A_{th} = 0.27 \pm 0.01$, $A_{th1} = 0.21 \pm 0.01$, $A_{th2} = 0.25 \pm 0.01$, $k_1 = (2.29 \pm 0.13) \times 10^7\ s^{-1}$, $k_2 = (2.80 \pm 0.40) \times 10^5\ s^{-1}$, $\beta_1 = 0.67 \pm 0.04$, and $\beta_2 = 0.40 \pm 0.02$. The time constant [$\tau_{th} = (2.40 \pm 0.02)$ μs] of the thermal decay part of the curve has been calibrated from diffraction grating measurements on malachite green (data shown in the inset). (From Walther, M., Raicu, V., Ogilvie, J. P., Phillips, R., Kluger, R., and Miller, R. J. D. 2005. *J. Phys. Chem. B* 109:20605–11. Used with permission.)

obtained both from fitting of the data with Equation (1.25) and from measurements on malachite green, which presents a pure thermal grating decay and thereby serves as a good reference for the analysis of phase grating data from MbCO. The transient-phase grating as well as the pump-probe absorption data of Walter et al. will be reanalyzed in the next subsection to extract physical information about the protein undergoing ligand photodissociation and geminate recombination.

C. Reanalysis of Data from Trehalose-Embedded MbCO

1. Extraction of the Distribution of Relaxation Functions from Experimental Data

One of the widely used methods of analysis of kinetic data is based on extraction of the distribution of relaxation times or, equivalently, enthalpic barrier heights. In this section, we show that this may be done easily by using the distribution function introduced by Raicu (1999; see Equation [1.16] above). To this end, we use the data reported by Walther and coworkers (Walther et al. 2005) from pump-probe as well as the transient phase grating measurements on trehalose-embedded MbCO. Their pump-probe data have been used without modification herein, while the phase grating data (also reproduced in Figure 1.12) have been corrected for thermal diffusion of the grating using the relaxation time reported above, τ_{th}, and Equation (1.25).

Equation (1.15) has been integrated numerically on a logarithmic scale to determine the dummy variable τ_{AB}. The logarithmic scale weighs more uniformly the relaxation times, which may cover several orders of magnitude. A change of variables, $y = \ln(k_p / k_{AB}) = \ln(\tau_{AB} / \tau_p)$, transformed the distribution function given by Equation (1.16) into the following function:

$$g(y) = \frac{1}{2\pi} \frac{e^{y\alpha}\sin[\pi(1-\beta)] + \mathrm{e}^{y(1-\beta)}\sin[\pi\alpha]}{\cosh[(1-\alpha-\beta)\mathrm{y}] + \cos[\pi(1-\alpha-\beta)]}. \tag{1.26}$$

The expression for the concentration profile given by Equation (1.15) has been accordingly replaced by

$$A(t) = \frac{\int_{y_{\min}}^{y_{\max}} g(y) e^{-\frac{t}{e^y \tau_p}} dy}{\int_{y_{\min}}^{y_{\max}} g(y) dy}. \tag{1.27}$$

where $y_{\min} = \ln(\tau_{\min} / \tau_p)$ and $y_{\max} = \ln(\tau_{\max} / \tau_p)$.

Equations (1.26) and (1.27) were used to fit the pump-probe and transient grating data from MbCO embedded in trehalose glass at room temperature, by assuming a symmetric cutoff for the relaxation times at low and high values (i.e., assuming that $y_{\min} = -y_{\max}$). This reduced the total number of fitting parameters to the following four: α, β, τ_p, and $\tau_{\max}$ (or $\tau_{\min}$). The goodness-of-fit was first evaluated by visually

TABLE 1.2
Best-Fit Parameter Values Corresponding to the Solid Lines in Figure 1.13

Measurement Method	τ_p (s)	α	β	τ_{max} (s)
Pump-probe	3.5×10^{-8}	0.08	0.14	8.54×10^{-5}
Transient grating	6.0×10^{-8}	0.06	0.15	6.53×10^{-2}

comparing the theoretical line to the experimental data, and then refining the parameter values to minimize a fitting residual given by the following expression:

$$\text{Residual} = \sum_i \frac{(A_{\text{theo},i} - A_{\text{exp},i})^2}{(A_{\text{exp},i})^2},$$

where i is a summation index ranging from 1 to the total number of time values. Figure 1.13 shows comparatively the experimental data and the best-fit curve, using the parameter values collected in Table 1.2.

In Figure 1.13 two recombination steps are clearly distinguishable, especially in the pump-probe data. These have been fitted previously by two separate stretched exponentials. Here, we used a single distribution of relaxation times, which accounted for both recombination steps.

Once the best-fit parameters are obtained, the distribution of relaxation times or, equivalently, barrier heights may be easily computed from Equation (1.16). The distribution function corresponding to the data in Figure 1.13 is plotted for the two types of measurements in Figure 1.14.

It is apparent from the above analysis that the most probable relaxation time, τ_p, for the transient phase grating is larger than the one for the pump-probe. While pump-probe absorption measurements report on changes in optical absorption accompanying ligand rebinding to the heme, the transient grating probes the structural changes in the entire protein. The longer relaxation time derived from the transient grating experiment therefore implies that the structural changes in the whole protein lag behind the formation of the iron–CO bond.

However, little more can be said about these differences without a detailed physical model at hand. Some physical significance of the data may be extracted by using a simple model proposed by Srajer, et al. (1988), as discussed below.

2. Determination of Certain Physical Parameters from Pump-Probe and Transient Grating Measurements

Srajer, Reinisch, and Champion (SRC) have proposed a model (Srajer et al. 1988; Srajer and Champion 1991), which separates the enthalpic barrier for ligand binding to the protein into the following two terms:

$$H = H_p + H_D = \frac{1}{2} K a^2 + H_D, \tag{1.28}$$

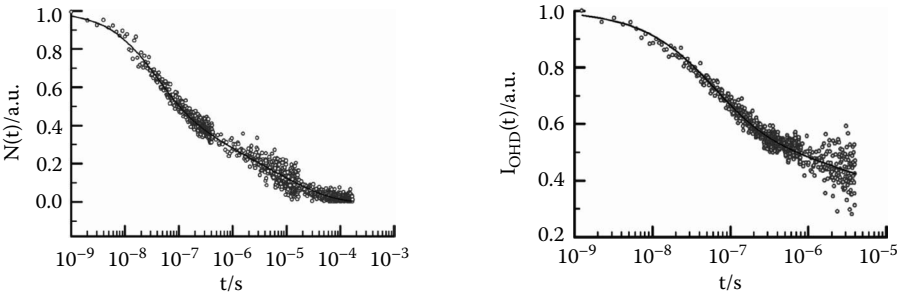

FIGURE 1.13 Experimental results (*points*) obtained from pump-probe (*left*) and transient phase grating (*right*) measurements of MbCO recombination as a function of time, *t*, following photodissociation. Solid lines were computed from equations (26) and (27), and the best-fit parameter values are listed in Table 1.2. (From Walther, M., Raicu, V., Ogilvie, J. P., Phillips, R., Kluger, R., and Miller, R. J. D. 2005. *J. Phys. Chem. B* 109:20605–11. With permission.)

where H_D takes into account the enthalpy barrier of the distal portions of the protein, and H_p describes the contributions to the enthalpic barrier from the heme distortions, which is necessary to bring the iron porphyrin system into the planar transition state configuration. The forces responsible for the displacement of the iron, *a*, to the in-plane geometry are modeled as a linear spring system, with *K* serving as an effective force constant (Srajer et al. 1988; Ye et al. 2007). In this model, the distribution of rate constants, or relaxation times, arises from the fact that there is a distribution of heme displacements, verified by x-ray studies. This distribution is assumed to be Gaussian in nature with a standard deviation σ_a around an equilibrium position a_0. Each enthalpic barrier of the distribution is associated with a different binding rate constant. The

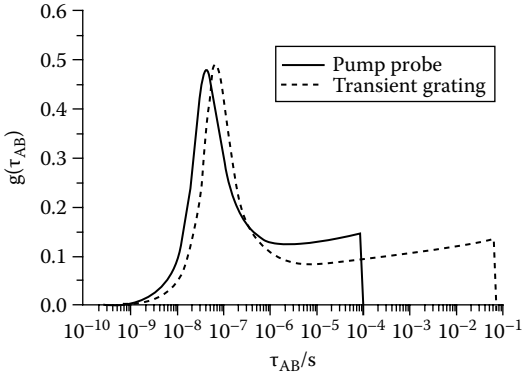

FIGURE 1.14 Distribution of relaxation times for the recombination of photodissociated Mb-CO.

displacement is related to the enthalpic barrier, as given by Equation (1.28), and the distribution of barrier heights can be written in the following form:

$$g(H) = \frac{1}{2\sigma_a[\pi K(H - H_D)]^{0.5}} \left[e^{-\frac{\left(\sqrt{H-H_D} - a_0\sqrt{\frac{K}{2}}\right)^2}{K\sigma_a^2}} + e^{-\frac{\left(\sqrt{H-H_D} + a_0\sqrt{\frac{K}{2}}\right)^2}{K\sigma_a^2}} \right], \quad (1.29)$$

where a_0 and σ_a^2 are the average and standard deviation of the assumed Gaussian distribution of the heme displacements. Similar to Equation (1.10), the concentration profile of bound ligands over time can be described by

$$A(t) = \int_{H_D}^{\infty} g(H) e^{\Omega t e^{\frac{-H}{k_B T}}} dH, \quad (1.30)$$

where it is assumed that $g(H)$ is zero when $H < H_D$.

For fitting purposes, a transformation of variables (Ye et al. 2007),

$$B = \sqrt{\frac{k_B T}{K\sigma_a^2}}, C = \frac{a_0}{\sqrt{2}\sigma_a}, t_0 = \frac{e^{\frac{H_D}{k_B T}}}{\Omega}, \text{ and } x = \frac{H - H_D}{k_B T}, \quad (1.31)$$

reduces the number of fitting parameters to just three. The concentration profile equation then becomes

$$A(t) = \int_0^{\infty} \frac{B}{2\sqrt{\pi x}} \left[e^{-\left(B\sqrt{x} - C\right)^2} + e^{-\left(B\sqrt{x} + C\right)^2} \right] e^{\frac{-t}{t_0} e^{-x}} dx. \quad (1.32)$$

We used this equation to fit the data obtained from the pump-probe and transient phase grating studies for MbCO in a trehalose glass discussed above. Plots of the experimental and simulated data are shown in Figure 1.15, while the parameters used to obtain the best-fit curve in the figure are listed in Table 1.3. Notice that, while the simulations based on the SRC model follow the general features of the curves in Figure 1.15, specific details (in particular the two steps, which were properly accounted for by Raicu's distribution function; see Figure 1.13) are not properly described by the SRC model. The precise reason for this is as yet unknown. The simplest, although admittedly the least spectacular, explanation would be the trapping of CO in different Xe pockets, wherefrom it recombines with the heme in two steps.

Equations (1.31) were solved to give

$$\sigma_a = \left(\frac{k_B T}{KB^2} \right)^{1/2}, \quad (1.33a)$$

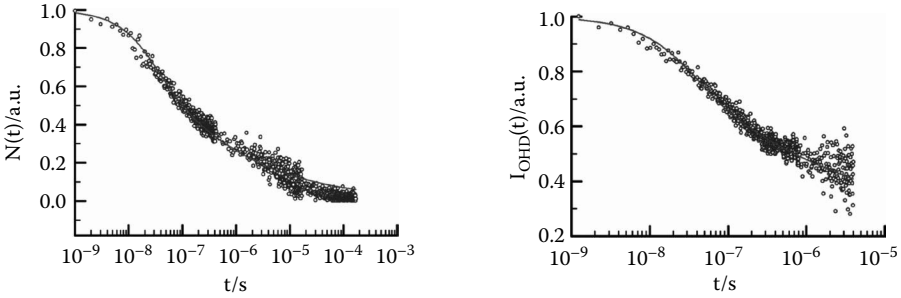

FIGURE 1.15 Reanalysis of the transient-grating and pump-probe data (*points*) of Walther et al. using the SRC model. Solid lines are theoretical simulations using equation (32) and the best-fit parameters given in Table 1.3. (From Walther, M., Raicu, V., Ogilvie, J. P., Phillips, R., Kluger, R., and Miller, R. J. D. 2005. *J. Phys. Chem. B.* 109:20605–11. With permission.)

$$a_0 = \left(\frac{2k_BT}{K}\right)^{1/2} \frac{C}{B}, \tag{1.33b}$$

$$\Omega = \frac{1}{t_0} \exp\left(\frac{H_D}{k_BT}\right), \tag{1.33c}$$

while the average $<H_p>$ is determined from its definition and using Equation (1.33b):

$$<H_p> = \frac{1}{2} K a_0^{\,2} = k_BT \left(\frac{C}{B}\right)^2. \tag{1.33d}$$

To determine the parameters a_0, σ_a, and H_p, we used the values for fitting parameters B and C (see above), the temperature $T = 293$ K and a spring constant, K, of 17 N/m (Srajer and Champion 1991). Further, by assuming a value of 18 kJ/mol for $H_p + H_D$ (Ye et al. 2007; Srajer et al. 1988), and using Equation (1.33c), the value of Ω was determined. All those values are listed in Table 1.4 along with results reported in previous publications, as follows: The first two rows of Table 1.4 list the results obtained from pump-probe and grating data obtained from MbCO embedded in a glass at room temperature (i.e., data from Figure 1.15). The third row lists the

TABLE 1.3
Best-Fit Parameters Obtained from Simulations of the Data in Figure 1.15 with the SRC Model [Equation (1.32)]

Sample	Method	t_0 (s)	B	C
MbCO	Pump-probe	1.1×10^{-8}	0.87	1.50
MbCO	Phase grating	2.6×10^{-8}	0.35	0.62

TABLE 1.4
Parameters Extracted from Fitting SRC Model to Data Obtained from MbCO as well as from the Protoheme Alone Embedded in Various Solvents

Sample	Method	Medium	T (K)	a_0 (Å)	σ_a (Å)	H_p (kJ/mol)	Ω (s^{-1})
MbCO[a]	Pump-probe	Trehalose	293	0.38	0.18	7.2	7.7×10^9
MbCO[a]	Phase grating	Trehalose	293	0.39	0.44	7.6	2.7×10^9
MbCO[b]	Flash photolysis	Glycerol	160	0.20	0.10	2.0	2.8×10^9
H_2O-FePPIXCO[c]	Pump-probe	Glycerol	293	0.27	0.11	6.0	1.5×10^{11}
H_2O-FePPIXCO[c]	Pump-probe	Glycerol	150	0.12	0.06	1.0	1.5×10^{11}

Note: The significance of the parameters and the methods used for their computation are described in the text.

[a] Data from Walther, M., Raicu, V., Ogilvie, J. P., Phillips, R., Kluger, R., and Miller, R. J. D. 2005. *J. Phys. Chem. B* 109:20605–11, analyzed as described above.

[b] Results from Srajer, V., and Champion, P. M. 1991. *Biochemistry* 30:7390–7402.

[c] Results from Ye, X., Ionascu, D., Gruia, F., Yu, A., Benabbas, A., and Champion, P. M. 2007. *Proc. Nat. Acad. Sci. USA* 104:14682–87.

parameters obtained from MbCO recombination studies performed in mixtures of glycerol and water at low temperatures (Srajer and Champion 1991). Finally, the last two rows correspond to studies of CO recombination to the bare protoheme (H_2O-FePPIXCO), i.e., in the absence of the protein (Ye et al. 2007).

It is interesting to note that the values of a_0 for MbCO in a room-temperature glass (trehalose) and in water-glycerol solvent at room temperatures are similar. The a_0 values obtained from the room-temperature studies agree well with those obtained from standard and time-resolved crystallographic studies comparing CO and deoxy structures of wild-type and mutant myoglobin (Vojtechovski et al. 1999; Kachalova et al. 1999; Nienhaus et al. 2005; Schmidt et al. 2005a), which range from 0.29 Å to 0.36 Å. Photoflash experiments on crystals at low temperatures show lower Fe displacements on the order of 0.1 Å to 0.2 Å (Schlichting et al. 1994; Teng et al. 1994, 1997; Hartmann et al. 1996). Similar values are also listed for the low temperature measurements in Table 1.4.

We also note that the values obtained for the prefactor Ω are the same for room-temperature and low-temperature glass; also, in both glasses, the values of Ω are about two orders of magnitude lower than in the case of bare protoheme. This latter difference was interpreted by Ye et al. (2007) as entropic control in the protein. This idea may be rationalized upon glancing at Equation (1.1), which predicts that, if not used explicitly in data analysis, a possible entropic contribution to the change in Gibbs free energy would be collected in the prefactor Ω.

Finally, the values of the proximal enthalpic barrier, H_p, are the same for trehalose-embedded protein and for the heme alone at room temperature, while at low temperatures both the Mb and the protoheme alone present similar H_p values. The equality between the proximal enthalpic barriers for the protein in liquid solvent and in a room-temperature glass may imply the existence of water in the trehalose-embedded MbCO, which may preserve the mobility of the protein (Librizzi et al. 2002).

ACKNOWLEDGMENTS

We thank Vukica Srajer for reading and commenting on an earlier version of the manuscript. V. R. and M. St. are supported by a UWM-RGI grant (X066), and M. Sch. is supported by the Deutsche Forschungsgemeinschaft (grant SCHM 1423/2-1).

REFERENCES

Amoros, J. L., Buerger, M. J., Canut de Amoros, M. 1975. *The Laue method*. New York: Academic Press.

Ansari, A., Jones, C. M., Henri, E. R., Hofrichter, J., and Eaton, W. A. 1992. The role of solvent viscosity in the dynamics of protein conformational changes. *Science* 256:1796–98.

Ansari, A., Jones, C. M., Henri, E. R., Hofrichter, J., and Eaton, W. A. 1994. Conformational relaxation and ligand binding in myoglobin. *Biochemistry* 33:5128–45.

Armstrong, M. R., Ogilvie, J. P., Cowan, M. L., Nagy, A. M., and Miller, R. J. D. 2003. Observation of the cascaded atomic-to-global length scales driving protein motion. *Proc. Nat. Acad. Sci. USA* 100:4990–4994.

Austin, R. H., Beeson, K. W., Eisenstein, L., Frauenfelder, H., and Gunsalus, I. C. 1975. Dynamics of ligand binding to myoglobin. *Biochemistry* 14:5355–73.

Bartunik, H. D., Bartsch, H. H., and Qichen, H. 1992. Accuracy in Laue x-ray diffraction analysis of protein structures. *Acta Crystallogr. A* 48:180–88.

Berman, H. M., Westbrook, J., Feng, Z., Gilliland, G., Bhat, T. N., Weissig, H., Shindyalov, I. N., and Bourne, P. E. 2000. The protein data bank. *Nucleic Acid Res.* 28:235–42.

Bourgeois, D., Vallone, B., Arcovito, A., Sciara, G., Schotte, F., Anfinrud, P. A., and Brunori, M. 2006. Extended subnanosecond structural dynamics of myoglobin revealed by Laue crystallography. *Proc. Natl. Acad. Sci. USA* 103:4924–29.

Bourgeois, D., Vallone, B., Schotte, F., Arcovito, A., Miele, A. E., Sciara, G., Wulff, M., Anfinrud, P., and Brunori, M. 2003. Complex landscape of protein structural dynamics unveiled by nanosecond Laue crystallography. *Proc. Natl. Acad. Sci. USA* 100:8704–9.

Carson, M. 1997. Ribbons. *Methods Enymol*. 277: 493–505.

Cohen, J., Arkhipov, A., Braun, R., and Schulten, K. 2006. Imaging the migration pathways for O_2, CO, NO, and Xe inside myoglobin. *Biophys. J*. 91:1844–57.

Cornish-Bowden, A. 1999. *Fundamentals of enzyme kinetics*, Revised Edition. London: Portland Press.

Dadusc, G., Ogilvie, J. P., Schulenberg, P., Marvet, U., and Miller, R. J. D. 2001. Diffractive optics-based heterodyne-detected four-wave mixing signals of protein motion: From "protein quakes" to ligand escape for myoglobin. *Proc. Nat. Acad. Sci. USA* 98:6110–6115.

Deak, J., Chiu, H. L., Lewis, C. M., and Miller, R. J. D. 1998. Ultrafast phase grating studies of heme proteins: Observation of the low-frequence modes directing functionally important protein motions, *J. Phys. Chem.* 102:6621–34.

Eichler, H. J., Gunter, P., and Pohl, D. W. 1986. *Laser-induced dynamic gratings*. Berlin: Springer-Verlag.

Eyring, H. 1935. The activated complex in chemical reactions. *J. Chem. Phys.* 3:107–15.

Fleck, G. M. 1971. *Chemical reaction mechanism*. New York: Holt, Rinehart and Winston.

Franzen, S., Bohn, B., Poyart, C., and Martin, J. L. 1995. Evidence for sub-picosecond heme doming in hemoglobin and myoglobin: A time-resolved resonance Raman comparison of carbonmonoxy and deoxy species. *Biochemistry* 34:1224–37.

Frauenfelder, H., Parak, F., and Young, R. D. 1988. Conformational substates in proteins. *Annu. Rev. Biophys. Biophys. Chem.* 17:451–79.

Goodno, G. D., Astinov, V., and Miller, R. J. D. 1999. Diffractive optics-based heterodyne-detected grating spectroscopy: Application to ultrafast protein dynamics. *J. Phys. Chem. A* 103:10619.

Goodno, G. D., Dadusc, G., and Miller, R. J. D. 1998. Ultrafast heterodyne-detected transient-grating spectroscopy using diffractive optics. *J. Opt. Soc. Am. B* 15:1791–94.

Hagen, S. J., and Eaton, W. A. 1996. Nonexponential structural relaxations in proteins. *J. Chem. Phys. B* 103:603–607.

Hagen, S. J., Hofrichter, W. A., and Eaton, W. A. 1995. Protein reaction-kinetics in a room-temperature glass. *Science* 269:959–62.

Hagen, S. J., Hofrichter, W. A., and Eaton, W. A. 1996. Geminate rebinding and conformational dynamics of myoglobin embedded in a glass at room temperature. *J. Phys. Chem.* 100:12008–21.

Hartmann, H., Zinser, S., Komninos, P., Schneider, R. T., Nienhaus, G. U., and Parak, F. 1996. X-ray structure determination of a metastable state of carbonmonoxy myoglobin after photodissociation. *Proc. Natl. Acad. Sci. USA* 93:7013–16.

Henderson, R., and Moffat, J. K. 1971. The difference Fourier technique in protein crystallography and their treatment. *Acta Crystallogr. B* 27:1414–20.

Henry, E. R., and Hofrichter, J. 1992. Singular value decomposition: Application to analysis of experimental data. *Meth. Enzymol*. 210:129–92.

Ihee, H., Rajagopal, S., Srajer, V., Pahl, R., Schmidt, M., Schotte, F., Anfinrud, P. A., Wulff, M., and Moffat, K. 2005. Visualizing chromophore isomerization in photoactive yellow protein from nanoseconds to seconds by time-resolved crystallography. *Proc. Natl. Acad. Sci., USA* 102:7145–50.

Jackson, T. A., Lim, M., and Anfinrud, P. A. 1994. Complex nonexponential relaxation in myoglobin after photodissociation of MbCO: Measurement and analysis from 2 ps to 56 ms. *Chemical Physics* 180:131–40.

Kachalova, G. S., Popov, A. N., and Bartunik, H. D. 1999. A steric mechanism for inhibition of CO binding to heme proteins. *Science* 284:473–76.

Kendrew, J. C., Bodo, G., Dintzis, H. M., Parrish, R. G., Wyckoff, H., and Phillips, D. C. 1958. A three-dimensional model of the myoglobin molecule obtained by X-ray analysis. *Nature* 181:662–66.

Kogelnik, H. 1969. Coupled wave theory for thick hologram gratings. *Bell Syst. Tech. J.* 48:2909–47.

Levenson, M. D., and Eesley, G. L. 1979. Polarization selective optical heterodyne detection for dramatically improved sensitivity in laser spectroscopy. *Appl. Phys.* 19:1–17.

Librizzi, F., Viapianni, C., Abbruzzetti, S., and Cordone, L. 2002. Residual water modulates the dynamics of the protein and of the external matrix in "trehalose-coated" MbCO: An infrared and flash-photolysis study. *J. Chem. Phys.* 116:1193–1200.

Lim, M., Jackson, T. A., and Anfinrud, P. A. 1993. Nonexponential protein relaxation: Dynamics of conformational change in myoglobin. *Proc. Natl. Acad. Sci. USA* 90:5801–4.

Matsen, F. A., and Franklin, J. L. 1950. A general theory of coupled sets of first order reactions. *J. Am. Chem. Soc.* 72:3337–41.

Miller, R. J. D. 2002. John C. Polany Award Lecture. Mother Nature and the molecular Big Bang. *Can. J. Chem.* 80:1–24.

Moffat, K. 1989. Time resolved macromolecular crystallography. *Annu. Rev. Biophys. Biophys. Chem.* 18:309–23.

Nagy, A., Raicu, V., and Miller, R. J. D. 2005. Nonlinear optical studies of heme protein dynamics: Implications for proteins as hybrid states of matter. *Biochim. Biophys. Acta* 1749:148–72.

Nelson, K. A., Miller, R. J. D., Lutz, D. R., and Fayer, M. D. 1982. Optical generation of tunable ultrasonic waves. *J. Appl. Phys.* 53:1144–49.

Nienhaus, K., Ostermann, A., Nienhaus, U., Parak, F., and Schmidt M. 2005. Ligand migration and protein fluctuations in myoglobin mutant L29W. *Biochemistry* 44:5095–5105.

Norrish, R. G. W. 1965. The kinetics and analysis of very fast chemical reactions. *Science* 149:1470–82.

Ogilvie, J. P., Armstrong, M. R., Plazanet, M., Dadusc, G., and Miller, R. J. D. 2001. Myoglobin dynamics: Evidence for a hybrid solid/fluid state of matter. *J. Luminesc.* 94-95:489–92.

Ogilvie, J. P., Plazanet, M., Dadusc, G., and Miller, R. J. D. 2002. Dynamics of ligand escape in myoglobin: Q-band transient absorption and four-wave mixing studies. *J. Phys. Chem.* 109:10460–67.

Ostermann, A., Waschipky, R., Parak, F. G., Nienhaus, G. U. 2000. Ligand binding and conformational motions in myoglobin. *Nature* 404:205–8.

Parak, F. G. 2003. Proteins in action: The physics of structural fluctuations and conformational changes. *Curr. Opin. Struct. Biol.* 13:552–57.

Parak, F., Knapp, E. W., and Kucheida, D. 1982. Protein dynamics. Mössbauer spectroscopy on deoxymyoglobin crystals. *J. Mol. Biol.* 161:177–94.

Raicu, V. 1999. Dielectric dispersion of biological matter: Model combining Debye-type and "universal" responses. *Phys. Rev. E* 60:4667–80.

Raicu, V., Sato, T., and Raicu, G. 2001. Non-Debye dielectric relaxation in biological structures arises from their fractal nature. *Phys. Rev. E* 64:021916.

Rajagopal, S., Anderson, S., Srajer, V., Schmidt, M., Pahl, R., and Moffat K. 2005. A structural pathway for signaling in the E46Q mutant of photoactive yellow protein. *Structure* 13:55–63.

Rajagopal, S., Schmidt, M., Anderson, S., and Moffat, K. 2004. Methodology for analysis of experimental time-resolved crystallographic data by singular value decomposition. *Acta Cryst*. D 60:860–71.

Ren, Z., Bourgeois, D., Helliwell, J. R., Moffat, K., Srajer, V., and Stoddard, B. L. 1999. Laue crystallography: Coming of age. *J. Synchrotron Rad*. 6:891–917.

Rogers, J. A., and Nelson, K. A. 1996. A new photoacoustic/photothermal device for real-time materials evaluation: An automated means for performing transient grating experiments. *Physica B* 56264:219–220.

Rovira, C., and Parrinello, M. 2000. First-principles molecular dynamics simulations of models of the myoglobin active center. *Int. J. Quantum Chem.* 80:1172–80.

Sakakura, M., Yamguchi, S., Horota, N., and Terazima, M. 2001. Dynamics of structure and energy of horse carboxymyoglobin after photodissociation of carbon monoxide. *J. Am. Chem. Soc.* 123:4286–94.

Sastry, G. M., and Agmon, N. 1997. Trehalose prevents myoglobin collapse and preserves its internal mobility. *Biochemistry* 36:7097–7108.

Schlichting, I., Berendzen, J., Phillips, G. N., and Sweet, R. M. 1994. Crystal structure of photolysed carbonmonoxy-myoglobin. *Nature* 371:808–12.

Schmidt, M. 2008. Structure based kinetics by time-resolved crystallography. In *Ultrashort laser pulses in biology and medicine*. M. Braun, P. Gilch, W. Zinth, Eds. New York: Springer Heidelberg.

Schmidt, M., Nienhaus, K., Pahl, R., Krasselt, A., Nienhaus, U., Parak, F., and Srajer, V. 2005a. Kinetic analysis of protein structural relaxations—A time-resolved crystallographic study. *Proc. Natl. Acad. Sci. USA* 13:11704–9.

Schmidt, M., Pahl, R., Ihee, H., and Srajer, V. 2005b. Protein ligand interactions probed by time-resolved X-ray structure determination. In *Methods in molecular biology, vol. 305: Protein-ligand interactions: Methods and Applications*. G. U. Nienhaus, Ed. Totowa, NJ: Humana Press.

Schmidt, M., Pahl, R., Srajer, V., Anderson, S., Ren, Z., Ihee, H., Rajagopal, S., and Moffat, K. 2004. Protein kinetics: Structures of intermediates and reaction mechanism from time-resolved X-ray data. *Proc. Natl. Acad. Sci. USA* 101:4799–4804.

Schmidt, M., Rajagopal, S., Ren, Z., and Moffat, K. 2003. Application of singular value decomposition to the analysis of time-resolved macromolecular x-ray data. *Biophys. J.* 84:2112–29.

Schotte, F., Lim, M., Jackson, T. A., Smirnov, A. V., Soman, J., Olson, J. S., Phillips, G. N. Jr., Wulff, M., and Anfinrud, P. A. 2003. Watching a protein as it functions with 150-ps time-resolved X-ray crystallography. *Science* 300:1944–47.

Schotte, F., Soman, J., Olson, J. S., Wulff, M., and Anfinrud, P. A. 2004. Picosecond time-resolved X-ray crystallography: Protein function in real time. *J. Struct. Biol.* 147:235–46.

Srajer, V., and Champion, P. M. 1991. Investigations of optical-line shapes and kinetic hole burning in myoglobin. *Biochemistry* 30:7390–7402.

Srajer, V., Reinisch, L., and Champion, P. M. 1988. Protein fluctuations, distributed coupling, and the binding of ligands to heme-proteins. *J. Am. Chem. Soc.* 110:6656–70.

Srajer, V., Ren, Z., Teng, T. Y., Schmidt, M., Ursby, T., Bourgeois, D., Pradervand, C., Schildkamp, W., Wulff, M., and Moffat, K. 2001. Protein conformational relaxation and ligand migration in myoglobin: Nanosecond to millisecond molecular movie from time-resolved Laue X-ray diffraction. *Biochemistry* 40:13802–15.

Srajer, V., Teng, T. Y., Ursby, T., Pradervand, C., Ren, Z., Adachi, S., Schildkamp, W., Bourgeois, D., Wulff, M., and Moffatt, K. 1996. Photolysis of the carbon monoxide complex of myoglobin: Nanosecond time-resolved crystallography. *Science* 274:1726–29.

Steinbach, P. J., Ansari, A., Berendzen, J., Braunstein, D., Chu K., Cowen, B. R. et al. 1991. Ligand binding to heme proteins: Connection between dynamics and function. *Biochemistry* 30:3988–4001.

Steinfeld, J. I., Francisco, J. S., and Hase, W. L. 1989. *Chemical kinetics and dynamics*. Englewood Cliffs, NJ: Prentice Hall.

Szebenyi, D. M. E., Bilderback, D. H., LeGrand, A., et al. 1992. Quantitative analysis of Laue diffraction pattern recorded with a 120 ps exposure from an X-ray undulator. *J. Appl. Cryst.* 25:414–23.

Teng, T. Y., Srajer, V., and Moffat, K. 1994. Photolysis-induced structural changes in single crystals of carbonmonoxy myoglobin at 40 K. *Struct. Biol.* 1:701–5.

Teng, T. Y., Srajer, V., and Moffat, K. 1997. Initial trajectory of carbon monoxide after photodissociation from myoglobin at cryogenic temperatures. *Biochemistry* 36:12087–12100.

Tian, W. D., Sage, J. T., Srajer, V., and Champion, P. M. 1992. Relaxation dynamics of myoglobin in solution. *Phys. Rev. Lett.* 68:408–11.

Tilton, R. F. Jr., Kuntz, I. D. Jr., and Petsko, G. A. 1984. Cavities in proteins: Structure of a metmyoglobin-xenon complex solved to 1.9 A. *Biochemistry* 23:2849–57.

Vojtechovsky, J., Chu, K., Berendzen, J., Sweet, R. M., and Schlichting, I. 1999. Crystal structures of myoglobin-ligand complexes at near-atomic resolution. *Biophys. J.* 77:2153–74.

Walther, M., Raicu, V., Ogilvie, J. P., Phillips, R., Kluger, R., and Miller, R. J. D. 2005. Determination of the Fe-CO bond energy in myoglobin using heterodyne-detected transient thermal phase grating spectroscopy. *J. Phys. Chem. B* 109:20605–11.

Ye, X., Ionascu, D., Gruia, F., Yu, A., Benabbas, A., and Champion, P. M. 2007. Temperature-dependent heme kinetics with nonexponential binding and barrier relaxation in the absence of protein conformational substates. *Proc. Nat. Acad. Sci. USA* 104:14682–87.